



THE UNIVERSITY *of* EDINBURGH

Edinburgh Research Explorer

## Helium-Iron Compounds at Terapascal Pressures

**Citation for published version:**

Monserrat, B, Martinez-Canales, M, Needs, RJ & Pickard, CJ 2018, 'Helium-Iron Compounds at Terapascal Pressures', *Physical Review Letters*, vol. 121, no. 01, pp. 015301.  
<https://doi.org/10.1103/PhysRevLett.121.015301>

**Digital Object Identifier (DOI):**

[10.1103/PhysRevLett.121.015301](https://doi.org/10.1103/PhysRevLett.121.015301)

**Link:**

[Link to publication record in Edinburgh Research Explorer](#)

**Document Version:**

Peer reviewed version

**Published In:**

Physical Review Letters

**General rights**

Copyright for the publications made accessible via the Edinburgh Research Explorer is retained by the author(s) and / or other copyright owners and it is a condition of accessing these publications that users recognise and abide by the legal requirements associated with these rights.

**Take down policy**

The University of Edinburgh has made every reasonable effort to ensure that Edinburgh Research Explorer content complies with UK legislation. If you believe that the public display of this file breaches copyright please contact [openaccess@ed.ac.uk](mailto:openaccess@ed.ac.uk) providing details, and we will remove access to the work immediately and investigate your claim.



# Helium-iron compounds at terapascal pressures

Bartomeu Monserrat,<sup>1,2,\*</sup> Miguel Martinez-Canales,<sup>3,4</sup> Richard J. Needs,<sup>2</sup> and Chris J. Pickard<sup>5,6</sup>

<sup>1</sup>*Department of Physics and Astronomy, Rutgers University, Piscataway, New Jersey 08854-8019, USA*

<sup>2</sup>*TCM Group, Cavendish Laboratory, University of Cambridge,  
J. J. Thomson Avenue, Cambridge CB3 0HE, United Kingdom*

<sup>3</sup>*Scottish Universities Physics Alliance, School of Physics and Astronomy,  
The University of Edinburgh, Edinburgh EH9 3FD, United Kingdom*

<sup>4</sup>*Centre for Science at Extreme Conditions, The University of Edinburgh, Edinburgh EH9 3FD, United Kingdom*

<sup>5</sup>*Department of Materials Science and Metallurgy, University of Cambridge,  
27 Charles Babbage Road, Cambridge CB3 0FS, United Kingdom*

<sup>6</sup>*Advanced Institute for Materials Research, Tohoku University 2-1-1 Katahira, Aoba, Sendai, 980-8577, Japan*  
(Dated: June 11, 2018)

We investigate the binary phase diagram of helium and iron using first-principles calculations. We find that helium, which is a noble gas and inert at ambient conditions, forms stable crystalline compounds with iron at terapascal pressures. A FeHe compound becomes stable above 4 TPa, and a FeHe<sub>2</sub> compound above 12 TPa. Melting is investigated using molecular dynamics simulations, and a superionic phase with sublattice melting of the helium atoms is predicted. We discuss the implications of our predicted helium-iron phase diagram for interiors of giant (exo)planets and white dwarf stars.

Matter under extreme compression exhibits rich and unexpected behaviour, such as unconventional chemistry [1, 2], structure [3], and phases [4]. Inside planets and stars, electrons and nuclei are subject to extreme conditions of pressure and temperature, and the exploration of new physics and chemistry under these conditions is necessary for the study of astrophysical processes within the interior of the Earth [5–7], other planets [8, 9], or stars [10–12].

Static experiments using diamond anvil cells have reached pressures of 1 terapascal (TPa, 1 TPa = 10<sup>7</sup> atmospheres) [13], well above those at the center of the Earth but smaller than those found at the cores of giant gas planets such as Jupiter and Saturn [14]. Higher pressures can be explored with dynamic compression experiments, as exemplified by the recent report from a team in the US National Ignition Facility that subjected diamond to pressures of 5 TPa [15, 16]. With high pressure experiments starting to investigate the realm of terapascal physics and chemistry, theoretical predictions are starting to emerge that reveal unexpected behaviour and complexity under these conditions.

In this context, we use quantum mechanical calculations to explore the phase diagram of helium and iron, two of the most abundant elements in the Universe.

Helium nuclei formed in the early Universe during Big Bang nucleosynthesis, and the primordial 25% mass fraction of helium makes it the second most abundant element after hydrogen. In addition, thermonuclear reactions within the interiors of stars fuse hydrogen to form helium. Therefore, helium is found inside many astrophysical objects, from planets, to stars, to white dwarf stars, and it plays a central role in their behaviour. For example, recent experimental and theoretical work has shown that helium metallises at TPa pressures [10–12], which is higher than previously anticipated. As a con-

sequence it has been suggested that the cooling rate of white dwarf stars is slowed by their helium-rich atmospheres, and therefore current estimates of their ages need to be revised.

Helium has two electrons in the closed-shell 1s state, and is chemically inert under ambient conditions. The only known helium compounds are either metastable, involving ionised species such as HeH<sub>2</sub><sup>+</sup> [17]; or are formed by weak van der Waals interactions, such as helium inside C<sub>60</sub> [18]. Recently, a helium-sodium compound has been reported above pressures of about 0.1 TPa [19].

Iron has one of the highest binding energies per nucleon (the highest is <sup>62</sup>Ni) and is therefore also very abundant [20]. It accounts for about 80% of the Earth's core mass [7], where it is found at pressures up to 0.35 TPa, and it is responsible for the magnetic field surrounding the planet [21]. Iron is not expected to exhibit magnetic order at TPa pressures, and it is predicted to occur in a series of closed-packed non-magnetic crystal structures [22]. Iron compounds with hydrogen, carbon, oxygen, silicon, and sulfur have been investigated at pressures of about 0.35 TPa due to their importance for the composition of the Earth's core [23].

In this work we investigate the possibility that, under extreme compression, helium might form stable compounds with iron. The high abundances of helium and iron make it crucial to understand the helium-iron phase diagram for astrophysical modelling of the interiors of giant planets, including the increasing number of exoplanets being discovered [24], and iron-core white dwarf stars [25].

Our strategy is to search for high-pressure compounds of helium and iron using first-principles quantum mechanical density functional theory (DFT) methods as implemented in the CASTEP code [26], and the *ab initio* random structure searching (AIRSS) method [27]. The

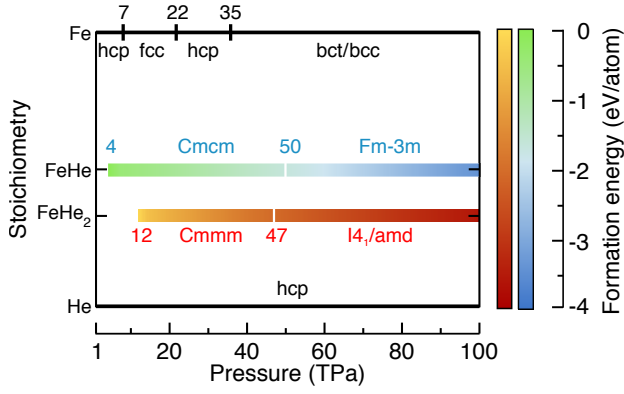


FIG. 1. Pressure-composition phase diagram of the helium-iron system at the static lattice level. For FeHe, the  $Cmc$  structure is stable between 4 and 50 TPa, and the  $Fm\bar{3}m$  structure above 50 TPa. For FeHe<sub>2</sub>, the  $Cmmm$  structure is stable between 12 and 47 TPa, and above that pressure the stable structure is  $I4_1/amd$ . The formation energy per atom, calculated using  $\Delta\mathcal{G}_s = (\mathcal{G}_s - (\mathcal{G}_{He}N_{He} + \mathcal{G}_{Fe}N_{Fe})) / (N_{He} + N_{Fe})$  as described in the text, is indicated by the gradients and approaches  $-4$  eV/atom for both stoichiometries at 100 TPa.

stability of a compound  $s$  with respect to the constituent elements can be evaluated by calculating the Gibbs free energy of formation per atom  $\Delta\mathcal{G}_s = (\mathcal{G}_s - (\mathcal{G}_{He}N_{He} + \mathcal{G}_{Fe}N_{Fe})) / (N_{He} + N_{Fe})$ , where  $\mathcal{G}_s$  is the Gibbs free energy of the compound  $s$ ,  $\mathcal{G}_A$  is the Gibbs free energy per atom of  $A$ , and  $N_A$  is the number of  $A$  atoms in compound  $s$ . The Gibbs free energy has contributions from the electrons, which we calculate using DFT, and from the quantum and thermal nuclear motion, which we calculate using DFT within the harmonic approximation together with the recently proposed nondiagonal supercell approach [28] which greatly reduces the computational cost. Further details of the calculations are provided in the Supplemental Material [29].

We show the static lattice phase diagram of the helium-iron system in the pressure range 1–100 TPa in Fig. 1. Helium is predicted to adopt the hexagonal closed-packed (hcp) crystal structure at TPa pressures [11]. Iron exhibits a sequence of phase transitions at TPa pressures, starting with the hcp structure which transforms to the face-centered cubic (fcc) structure in the range 7–22 TPa, then it transforms back to the hcp structure up to pressures of 35 TPa, above which it transforms into the body-centered tetragonal (bct) structure, which approaches the body-centered cubic (bcc) structure with increasing pressure [22, 30].

The structure searches find several compounds of helium and iron that are energetically competitive in the TPa pressure range, and the most stable have stoichiometries FeHe and FeHe<sub>2</sub> (see Fig. 1). The FeHe stoichiometry first forms at 4 TPa in a structure of orthorhombic space group  $Cmc$  containing 8 atoms in the primitive cell, and at 50 TPa it transforms to a  $Fm\bar{3}m$  structure

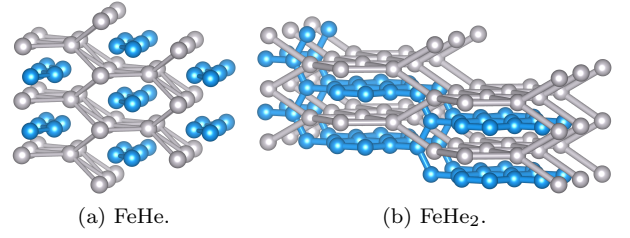


FIG. 2. Crystal structures of  $Cmc$  FeHe and  $Cmmm$  FeHe<sub>2</sub> at 10 TPa. Helium atoms are represented in blue, and iron atoms in grey.

(rock-salt structure). The FeHe<sub>2</sub> stoichiometry appears in three distinct structures which have similar energies. The first is an orthorhombic structure of space group  $Cmmm$  with nine atoms in the primitive cell, which forms around 12 TPa. The second has a space group of  $I4_1/amd$  symmetry with six atoms in the primitive cell, and becomes the most stable FeHe<sub>2</sub> structure above 47 TPa. The third has  $P6_3/mmm$  space group and three atoms in the primitive cell, but is not thermodynamically stable. Structure files for all of the helium-iron compounds are provided as Supplemental Material [29].

The helium-iron compounds that form at the lowest pressures have the FeHe  $Cmc$  and the FeHe<sub>2</sub>  $Cmmm$  structures shown in Fig. S4. The iron atoms form open channels containing helium chains in the FeHe  $Cmc$  structure (Fig. S4a). At 10 TPa, the minimum He-He distance is 0.98 Å, the He-Fe distance is 1.16 Å, and the Fe-Fe distance is 1.47 Å. The volume per formula unit in FeHe is 2.76 Å<sup>3</sup>, compared to 0.50 Å<sup>3</sup> in hcp helium and 2.27 Å<sup>3</sup> in both hcp and fcc iron, which add to a combined volume of 2.77 Å<sup>3</sup> per formula unit. In the FeHe<sub>2</sub>  $Cmmm$  structure (Fig. S4c), the helium atoms form hexagonal layers incorporated inside iron channels that are wider than those present in FeHe. The minimum He-He distance is 0.89 Å at 10 TPa, the He-Fe distance is 1.19 Å, and the Fe-Fe distance is larger at 1.54 Å. The volume per formula unit in FeHe<sub>2</sub> is 3.24 Å<sup>3</sup>, which is smaller than that of the elements (total of 3.27 Å<sup>3</sup>). The smaller volumes of the compounds favour their formation under pressure via the enthalpy term in the Gibbs free energy.

We next investigate the effects of temperature on the formation of helium-iron compounds upon increasing pressure. If the effects of nuclear motion are neglected, FeHe forms at pressures above 4.1 TPa, and the inclusion of quantum and thermal nuclear motion lowers this pressure to 2.7 TPa at 10,000 K. FeHe<sub>2</sub> only forms at a higher pressure of about 12 TPa, and therefore we focus on the FeHe compound to study the formation of helium-iron compounds under pressure.

We use *ab initio* molecular dynamics simulations in conjunction with the Z-method [31] to estimate the melting temperature of FeHe. These calculations are

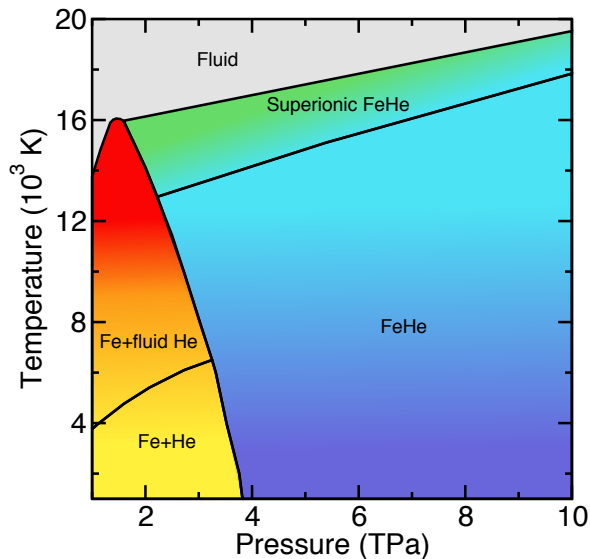


FIG. 3. Helium-iron phase diagram. The solid lines indicate formation lines, sublattice melting, and full melting. The sublattice melting of FeHe occurs at  $15,100 \pm 1,000$  K at 5.38 TPa, and at  $18,200 \pm 1,000$  K at 10.6 TPa, while the full melting of FeHe occurs at  $17,600 \pm 1,000$  K at 5.45 TPa, and at  $19,800 \pm 1,000$  K at 10.65 TPa. The melting line of iron is taken from Ref. [36].

performed using the QUANTUM ESPRESSO package [32], and the details are provided in the Supplemental Material [29]. The melting temperatures of helium and iron differ by thousands of degrees, suggesting that FeHe might exhibit superionicity, that is, sublattice melting of the helium component while the iron atoms oscillate around their crystallographic positions. Superionicity has been discussed before [33], for example in a lithium-based conductor at ambient pressure [34], and in the melting of ice and ammonia at extreme pressures [8]. Indeed, our molecular dynamics simulations demonstrate that, upon increasing temperature, the helium chains melt within the iron channels in FeHe before the iron channels themselves melt. Interestingly, metallic superionic compounds are uncommon [35], and FeHe provides a nice platform to further investigate their properties.

In Fig. 3 we show the proposed phase diagram for the formation of helium-iron compounds under pressures up to 10 TPa. At low pressures, helium and iron do not mix. Below about 4,000 K at 1 TPa and 6,000 K at 3 TPa, both materials are found in the solid state, but helium melts above this temperature. Iron only melts at much higher temperatures, of the order of 15,000 K [36]. Upon increasing pressure, helium and iron form a FeHe compound between 2 and 4 TPa, depending on the temperature. FeHe undergoes sublattice melting of the helium atoms at temperatures between 13,000 and 18,000 K, depending on the pressure. The superionic phase is stable in a wide temperature and pressure range, and melting

is completed at around 17,000 K at 4 TPa, and above 19,000 K at 10 TPa.

Our results suggest that the FeHe compound should form at the pressures accessible to dynamic compression experiments. Furthermore, the formation pressure of FeHe is predicted to be within the pressure range found at the core of Jupiter, with a core-mantle boundary pressure of 4.2 TPa and temperature of 20,000 K, and at the highest pressures found at the centre of Saturn, with a core-mantle boundary pressure of 1 TPa [14, 37]. The interiors of exoplanets with masses similar or larger than that of Jupiter will also be subject to pressures higher than those required to form FeHe. This raises the possibility that helium is captured by iron within the interior of these planets, and potentially bound to other elements. The atmosphere of Saturn is indeed depleted of helium [38], and the capture of helium in compounds in its interior could contribute to this phenomenon. This could also affect the helium composition of the atmospheres of giant exoplanets. White dwarf stars are subject to more extreme conditions, with helium-rich atmospheres subject to tens of terapascals, and the interiors to even higher pressures. Due to cooling, white dwarf stars exhibit temperatures in the range from only a few thousand Kelvin to hundreds of thousand of Kelvin [39], raising the possibility that even the solid FeHe phases appear in these stars. The formation of helium compounds with other elements could alter the cooling rates of white dwarf stars, which are largely determined by the atmospheric composition, and as a consequence affect current estimates of their ages. Our results indicate that, in contrast to the inertness of helium at ambient pressure, accurate models of the composition of planets and stars should treat helium as a compound-forming element.

In conclusion, we have used first-principles methods to study the binary phase diagram of helium and iron. We have found that compounds can form at pressures of several TPa, suggesting that they might be found inside giant (exo)planets and white dwarf stars. We have also predicted that the most stable FeHe compound exhibits a superionic phase with sublattice melting of the helium atoms within a wide range of temperatures and pressures. Overall, our results show that helium can form compounds at terapascal pressures.

B.M. acknowledges support from the Winton Programme for the Physics of Sustainability, and from Robinson College, Cambridge, and the Cambridge Philosophical Society for a Henslow Research Fellowship. R.J.N. and C.J.P. acknowledge financial support from the Engineering and Physical Sciences Research Council (EPSRC) of the UK [EP/J017639/1 and EP/G007489/2]. C.J.P. is also supported by the Royal Society through a Royal Society Wolfson Research Merit award. The calculations were performed on the Cambridge High Performance Computing Service facility and the Archer facility of the UK's national high-



performance computing service (for which access was obtained via the UKCP consortium [EP/K014560/1 and EP/K013688/1]).

---

\* [bm418@cam.ac.uk](mailto:bm418@cam.ac.uk)

- [1] Chris J. Pickard, Miguel Martinez-Canales, and Richard J. Needs, “Decomposition and terapascal phases of water ice,” *Phys. Rev. Lett.* **110**, 245701 (2013).
- [2] S. Ninet, F. Datchi, P. Dumas, M. Mezouar, G. Garbarino, A. Mafey, C. J. Pickard, R. J. Needs, and A. M. Saitta, “Experimental and theoretical evidence for an ionic crystal of ammonia at high pressure,” *Phys. Rev. B* **89**, 174103 (2014).
- [3] D. Kobayakov and C. J. Pethick, “Towards a metallurgy of neutron star crusts,” *Phys. Rev. Lett.* **112**, 112504 (2014).
- [4] A. P. Drozdov, M. I. Erements, I. A. Troyan, V. Ksenofontov, and S. I. Shylin, “Conventional superconductivity at 203 kelvin at high pressures in the sulfur hydride system,” *Nature* **525**, 73 (2015).
- [5] D. Alfè, M. J. Gillan, and G. D. Price, “The melting curve of iron at the pressures of the Earth’s core from *ab initio* calculations,” *Nature* **401**, 462 (1999).
- [6] Monica Pozzo, Chris Davies, David Gubbins, and Dario Alfè, “Thermal and electrical conductivity of iron at Earth’s core conditions,” *Nature* **485**, 355 (2012).
- [7] Christopher Davies, Monica Pozzo, David Gubbins, and Dario Alfè, “Constraints from material properties on the dynamics and evolution of Earth’s core,” *Nature Geosci.* **8**, 678 (2015).
- [8] C. Cavazzoni, G. L. Chiarotti, S. Scandolo, E. Tosatti, M. Bernasconi, and M. Parrinello, “Superionic and metallic states of water and ammonia at giant planet conditions,” *Science* **283**, 44–46 (1999).
- [9] Hugh F. Wilson, Michael L. Wong, and Burkhard Militzer, “Superionic to superionic phase change in water: Consequences for the interiors of Uranus and Neptune,” *Phys. Rev. Lett.* **110**, 151102 (2013).
- [10] S. A. Khairallah and B. Militzer, “First-principles studies of the metallization and the equation of state of solid helium,” *Phys. Rev. Lett.* **101**, 106407 (2008).
- [11] Bartomeu Monserrat, N. D. Drummond, Chris J. Pickard, and R. J. Needs, “Electron-phonon coupling and the metallization of solid helium at terapascal pressures,” *Phys. Rev. Lett.* **112**, 055504 (2014).
- [12] R. Stewart McWilliams, D. Allen Dalton, Zuzana Konpkov, Mohammad F. Mahmood, and Alexander F. Goncharov, “Opacity and conductivity measurements in noble gases at conditions of planetary and stellar interiors,” *Proc. Natl. Acad. Sci. USA* **112**, 7925–7930 (2015).
- [13] Natalia Dubrovinskaia, Leonid Dubrovinsky, Natalia A. Solopova, Artem Abakumov, Stuart Turner, Michael Hanfland, Elena Bykova, Maxim Bykov, Clemens Prescher, Vitali B. Prakapenka, Sylvain Petitgirard, Irina Chuvashova, Biliana Gasharova, Yves-Laurent Mathis, Petr Ershov, Irina Snigireva, and Anatoly Snigirev, “Terapascal static pressure generation with ultrahigh yield strength nanodiamond,” *Sci. Adv.* **2** (2016).
- [14] W. B. Hubbard and B. Militzer, “A preliminary Jupiter model,” *Astrophys. J.* **820**, 80 (2016).
- [15] R. F. Smith, J. H. Eggert, R. Jeanloz, T. S. Duffy, D. G. Braun, J. R. Patterson, R. E. Rudd, J. Biener, A. E. Lazicki, A. V. Hamza, J. Wang, T. Braun, L. X. Benedict, P. M. Celliers, and G. W. Collins, “Ramp compression of diamond to five terapascals,” *Nature* **511**, 330 (2014).
- [16] Chris J. Pickard and Richard J. Needs, “High-pressure physics: Piling on the pressure,” *Nature* **511**, 294 (2014).
- [17] T. R. Hogness and E. G. Lunn, “The ionization of hydrogen by electron impact as interpreted by positive ray analysis,” *Phys. Rev.* **26**, 44–55 (1925).
- [18] Martin Saunders, Hugo A. Jiménez-Vázquez, R. James Cross, and Robert J. Poreda, “Stable compounds of helium and neon: He@C60 and Ne@C60,” *Science* **259**, 1428–1430 (1993).
- [19] Xiao Dong, Artem R. Oganov, Alexander F. Goncharov, Elissaios Stavrou, Sergey Lobanov, Gabriele Saleh, Guang-Rui Qian, Qiang Zhu, Carlo Gatti, Volker L. Deringer, Richard Dronskowski, Xiang-Feng Zhou, Vitali B. Prakapenka, Z. Konôpková, Ivan A. Popov, Alexander I. Boldyrev, and Hui-Tian Wang, “A stable compound of helium and sodium at high pressure,” *Nat. Chem.* **9**, 440 (2017).
- [20] E. Margaret Burbidge, G. R. Burbidge, William A. Fowler, and F. Hoyle, “Synthesis of the elements in stars,” *Rev. Mod. Phys.* **29**, 547–650 (1957).
- [21] Bruce A. Buffett, “Earth’s core and the geodynamo,” *Science* **288**, 2007–2012 (2000).
- [22] C. J. Pickard and R. J. Needs, “Stable phases of iron at terapascal pressures,” *J. Phys. Condens. Matter* **21**, 452205 (2009).
- [23] Jean-Paul Poirier, “Light elements in the Earth’s outer core: A critical review,” *Phys. Earth Planet. Inter.* **85**, 319 – 337 (1994).
- [24] Michel Mayor, Christophe Lovis, and Nuno C. Santos, “Doppler spectroscopy as a path to the detection of Earth-like planets,” *Nature* **513**, 328 (2014).
- [25] George C. Jordan IV, Hagai B. Perets, Robert T. Fisher, and Daniel R. van Rossum, “Failed-detonation supernovae: Subluminous low-velocity Ia supernovae and their kicked remnant white dwarfs with iron-rich cores,” *The Astrophysical Journal Letters* **761**, L23 (2012).
- [26] Stewart J. Clark, Matthew D. Segall, Chris J. Pickard, Phil J. Hasnip, Matt I. J. Probert, Keith Refson, and Mike C. Payne, “First principles methods using CASTEP,” *Z. Kristallogr.* **220**, 567 (2005).
- [27] Chris J. Pickard and R. J. Needs, “*Ab initio* random structure searching,” *J. Phys. Condens. Matter* **23**, 053201 (2011).
- [28] Jonathan H. Lloyd-Williams and Bartomeu Monserrat, “Lattice dynamics and electron-phonon coupling calculations using nondiagonal supercells,” *Phys. Rev. B* **92**, 184301 (2015).
- [29] See Supplemental Material at [...] for numerical details of the first principles calculations and for cif files for the FeHe and FeHe<sub>2</sub> structures. It includes Refs. [40–42].
- [30] Lars Stixrude, “Structure of iron to 1 Gbar and 40 000 K,” *Phys. Rev. Lett.* **108**, 055505 (2012).
- [31] A. B. Belonoshko, N. V. Skorodumova, A. Rosengren, and B. Johansson, “Melting and critical superheating,” *Phys. Rev. B* **73**, 012201 (2006).
- [32] Paolo Giannozzi, Stefano Baroni, Nicola Bonini, Matteo Calandra, Roberto Car, Carlo Cavazzoni, Davide Ceresoli, Guido L. Chiarotti, Matteo Cococcioni, Ismaila Dabo, Andrea Dal Corso, Stefano de Gironcoli, Ste-

- fano Fabris, Guido Fratesi, Ralph Gebauer, Uwe Gerstmann, Christos Gougoussis, Anton Kokalj, Michele Lazzeri, Layla Martin-Samos, Nicola Marzari, Francesco Mauri, Riccardo Mazzarello, Stefano Paolini, Alfredo Pasquarello, Lorenzo Paulatto, Carlo Sbraccia, Sandro Scandolo, Gabriele Sclauser, Ari P Seitsonen, Alexander Smogunov, Paolo Umari, and Renata M Wentzcovitch, “QUANTUM ESPRESSO: a modular and open-source software project for quantum simulations of materials,” *J. Phys.: Condens. Matter* **21**, 395502 (2009).
- [33] Stephen Hull, “Superionics: crystal structures and conduction processes,” *Rep. Prog. Phys.* **67**, 1233 (2004).
- [34] Noriaki Kamaya, Kenji Homma, Yuichiro Yamakawa, Masaaki Hirayama, Ryoji Kanno, Masao Yonemura, Takashi Kamiyama, Yuki Kato, Shigenori Hama, Koji Kawamoto, and Akio Mitsui, “A lithium superionic conductor,” *Nat. Mater.* **10**, 682 (2011).
- [35] Martin French, Thomas R. Mattsson, and Ronald Redmer, “Diffusion and electrical conductivity in water at ultrahigh pressures,” *Phys. Rev. B* **82**, 174108 (2010).
- [36] G. Morard, J. Bouchet, D. Valencia, S. Mazevet, and F. Guyot, “The melting curve of iron at extreme pressures: Implications for planetary cores,” *High Energy Density Phys.* **7**, 141–144 (2011).
- [37] N. Nettelmann, A. Becker, B. Holst, and R. Redmer, “Jupiter models with improved ab initio hydrogen equation of state (H-REOS.2),” *Astrophys. J.* **750**, 52 (2012).
- [38] D. J. Stevenson, “Saturn’s luminosity and magnetism,” *Science* **208**, 746–748 (1980).
- [39] Brad M.S. Hansen and James Liebert, “Cool white dwarfs,” *Annu. Rev. Astron. Astrophys.* **41**, 465–515 (2003).
- [40] John P. Perdew, Kieron Burke, and Matthias Ernzerhof, “Generalized gradient approximation made simple,” *Phys. Rev. Lett.* **77**, 3865 (1996).
- [41] Chris J. Pickard and R. J. Needs, “High-pressure phases of silane,” *Phys. Rev. Lett.* **97**, 045504 (2006).
- [42] K. Kunc and Richard M. Martin, “*Ab Initio* force constants of GaAs: A new approach to calculation of phonons and dielectric properties,” *Phys. Rev. Lett.* **48**, 406–409 (1982).

# Supplemental Material for “Helium-iron compounds at terapascal pressures”

## COMPUTATIONAL DETAILS

### Density functional theory

Density functional theory calculations have been performed using the plane-wave pseudopotential CASTEP code [S26] with the PBE functional [S40]. The extreme pressures we study force us to use tailored pseudopotentials with core radii of 0.6 bohr for helium and 1.0 bohr for iron, and our calculations explicitly include the 1s states of helium and the 3s3p3d4s states of iron. The pseudopotential strings used are:

```
He 1|0.6|27|31|36|10(qc=11)
Fe 3|1.0|33|38|44|30U:40:31:32(qc=11)
```

These hard pseudopotentials require plane-wave cut-off energies of 1500 eV. For the searches we have used Brillouin zone  $\mathbf{k}$ -point grids of density  $2\pi \times 0.07 \text{ \AA}^{-1}$ , and finer grids of density  $2\pi \times 0.025 \text{ \AA}^{-1}$  for the final results and the vibrational calculations. Structures were relaxed to achieve uncertainties in the pressure below 0.1 TPa.

### AIRSS

The structure searches have been performed using the AIRSS method [S27, S41] at pressures of 5 TPa, 10 TPa, and 50 TPa, and with stoichiometries  $\text{Fe}_x\text{He}_y$  for  $x, y = 1, \dots, 6$ . The total number of structures generated in the searches is 7,371.

### Vibrational calculations

Harmonic vibrational free energies have been calculated using finite-displacements [S42] with the nondiagonal supercells method [S28]. The system sizes required to obtain converged results are shown in Table I, and the accuracy required could not have been achieved unless nondiagonal supercells had been used, as the computational cost of using small radii pseudopotentials is significant. Results accurate to 1 meV/atom have been obtained by diagonalising the corresponding dynamical matrices over a fine vibrational Brillouin-zone grid. Anharmonic vibrations have been previously found to be negligible in helium at TPa pressures [S11].

TABLE I. Size of largest supercell required for the corresponding vibrational BZ grid.

	BZ grid size	Diagonal supercells	Nondiagonal supercells
He-hpc	$4 \times 4 \times 4$	64 cells (128 atoms)	4 cells (8 atoms)
Fe-hcp	$4 \times 4 \times 4$	64 cells (128 atoms)	4 cells (8 atoms)
Fe-fcc	$4 \times 4 \times 4$	64 cells (64 atoms)	4 cells (4 atoms)
FeHe- <i>Cmcm</i>	$3 \times 3 \times 3$	27 cells (216 atoms)	3 cells (24 atoms)
FeHe <sub>2</sub> - <i>P6/mmm</i>	$5 \times 5 \times 5$	125 cells (375 atoms)	5 cells (15 atoms)
FeHe <sub>2</sub> - <i>I4<sub>1</sub>/amd</i>	$3 \times 3 \times 3$	27 cells (162 atoms)	3 cells (18 atoms)
FeHe <sub>2</sub> - <i>Cmmm</i>	$4 \times 4 \times 4$	64 cells (576 atoms)	4 cells (36 atoms)

## THERMODYNAMIC STABILITY

In this section we show the relative stability of the various crystal structures for iron, helium, FeHe, and FeHe<sub>2</sub>. For any pressure-temperature conditions, the thermodynamically stable structure is used in the main text.

The relevant structures of iron are the face-centered cubic (fcc), body-centered cubic (bcc), body-centered tetragonal (bct), and hexagonal closed-packed (hcp). Their relative static lattice enthalpies are shown in Fig. S1a. In agreement

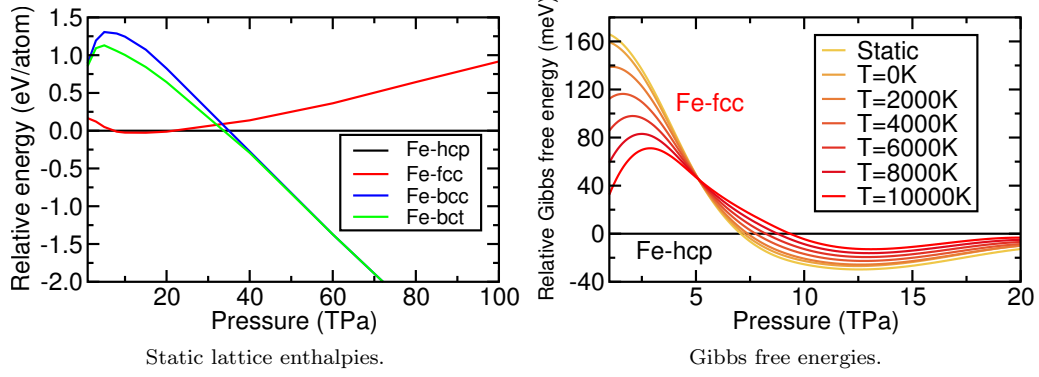


FIG. S1. Relative enthalpies and Gibbs free energies of fcc and bcc iron with respect to hcp iron.

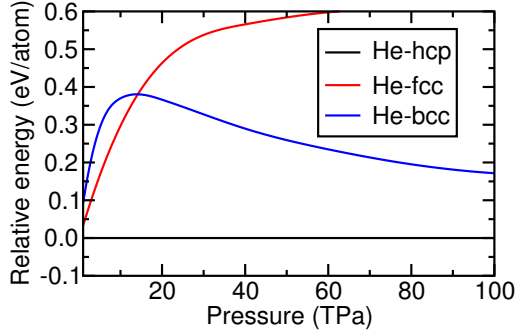


FIG. S2. Relative enthalpies of fcc and bcc helium with respect to hcp helium.

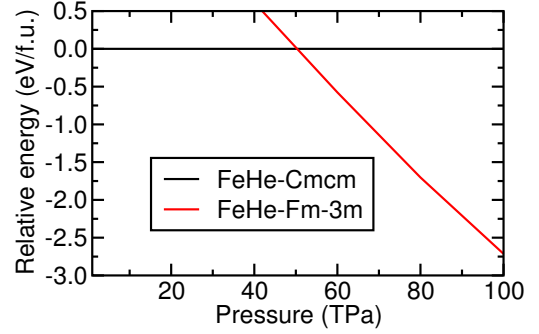


FIG. S3. Relative enthalpies of FeHe-*Cmcm* and FeHe-*Fm-3m*.

with previous reports [S22], we find that fcc iron becomes stable compared to hcp iron at pressures in the range 7.4 TPa to 21.7 TPa, and a body-centered tetragonal (bct) iron is the most stable structure above 35 TPa. The bct structure approaches the bcc structure with increasing pressure. The effects of temperature are shown in Fig. S1b up to 20 TPa. Including quantum and thermal nuclear motion destabilises fcc iron, so that at 10,000 K it only becomes stable at 9.4 TPa.

Helium is only found in the hcp structure in the entire pressure range from 1 TPa to 100 TPa. A comparison with the bcc and fcc structures is provided in Fig. S2.

For the helium-iron FeHe stoichiometry, there are two different structures that are energetically competitive: (i) a structure of space group *Cmcm* with 8 atoms in the primitive cell, and (ii) a structure of space group *Fm $\bar{3}m$*  with 2 atoms in the primitive cell (rock-salt structure). The relative enthalpies of these structures are shown in Fig. S3.

For the helium-iron FeHe<sub>2</sub> stoichiometry, there are three different structures that are energetically competitive: (i)

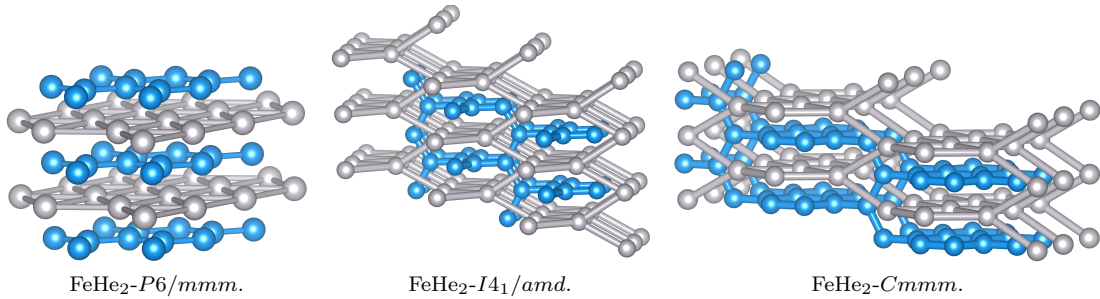


FIG. S4. Crystal structures of *P6/mmm* FeHe<sub>2</sub>, *I4<sub>1</sub>/amd* FeHe<sub>2</sub>, and *Cmmm* FeHe<sub>2</sub> at 10 TPa. Helium atoms are represented in blue, and iron atoms in grey.



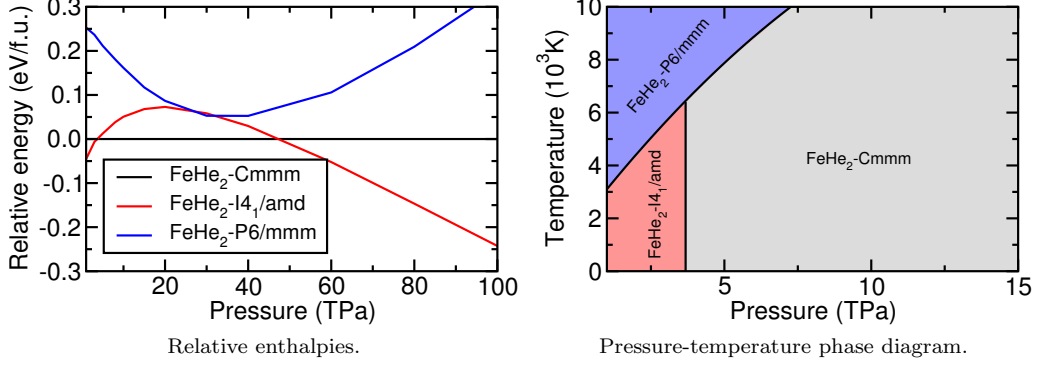


FIG. S5. Phase diagram for the helium-iron compounds of  $\text{FeHe}_2$  stoichiometry.

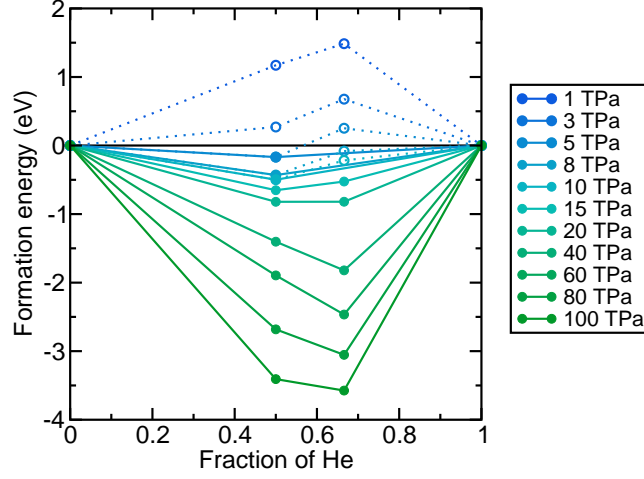


FIG. S6. Convex hull diagram for the helium-iron system at the static lattice level and for a range of temperatures. The solid circles indicate structures on the convex hull, and the solid lines connect them. The open circles indicate structures that are not on the convex hull, and these are connected by dotted lines as a guide to the eye.

a structure of space group  $P6/mmm$  with 3 atoms in the primitive cell, (ii) a structure of space group  $I4_1/amd$  with 6 atoms in the primitive cell, and (iii) a structure of space group  $Cmmm$  with 9 atoms in the primitive cell. These structures are depicted in Fig. S4, and their relative enthalpies and low pressure phase diagram are shown in Fig. S5. Combining the He, Fe, FeHe, and  $\text{FeHe}_2$  results, we construct the convex hull diagram for the helium-iron mixtures, shown in Fig. S6.

## SUPERIONICITY AND MELTING

We investigate superionicity and melting in the FeHe  $Cmcm$  structure using molecular dynamics simulations performed with QUANTUM ESPRESSO [S32]. We used pseudopotentials converted from CASTEP with the following strings:

```
He 1|0.7|27|31|36|10(qc=9.2)
Fe 3|1.2|30|35|40|30U:40:31:32(qc=10)
```

We note that the computational expense of the molecular dynamics calculations forced us to use pseudopotentials with larger core radii than those used for the lattice dynamics calculations. Nonetheless, we have calculated the phonon density of states at 10 TPa for the FeHe  $Cmcm$  structure and confirmed that the hard and soft pseudopotentials lead to consistent results (see Fig. S7). We used an energy cutoff of 90 Ry (1225 eV), and a charge density cutoff of 720 Ry. The electronic Brillouin zone was sampled using a  $2 \times 2 \times 2$   $\mathbf{k}$ -point grid for a  $4 \times 2 \times 4$  supercell of the conventional cell of the  $Cmcm$  structure, containing a total of 256 atoms.

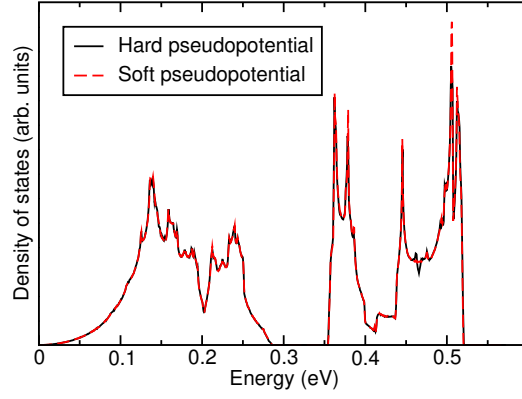


FIG. S7. Phonon vibrational density of states for FeHe at 10 TPa using a vibrational BZ grid of size  $3 \times 3 \times 3$  and Fourier interpolation.

The molecular dynamics simulations were used to investigate the melting curve of the FeHe *Cmcm* compound, for which the Z-method [S31] was used. In this method, the temperature is increased to the desired value using an NVT ensemble, and then relaxed using an NVE ensemble. This procedure is iterated while checking whether a component (He or Fe) is diffusing or the whole lattice has melted by monitoring both the temperature and the mean square displacement (MSD) of the relevant species. Representative runs at 5 and 10 TPa are shown in Fig. S8.

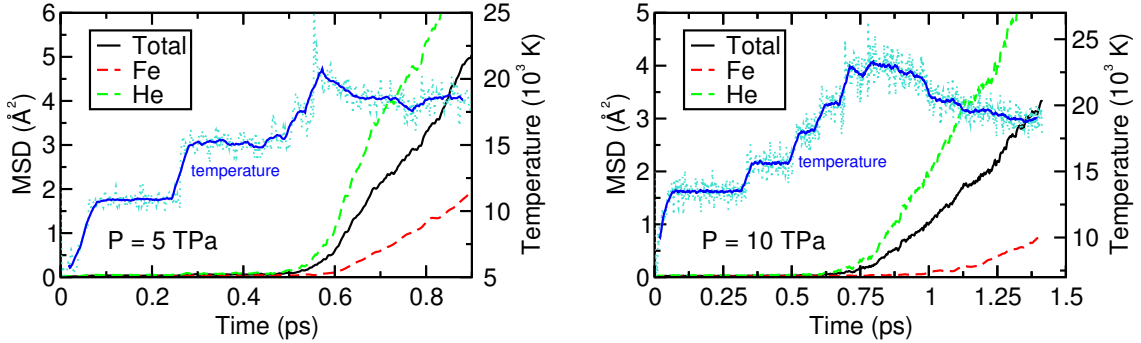


FIG. S8. Molecular dynamics runs of *Cmcm* FeHe. The MSD for the individual Fe and He atoms, as well as the combined MSD are shown on the left vertical axis. The temperature is shown on the right vertical axis, with the blue solid line representing the average over 50 points, and the light blue dotted line the instantaneous temperature.

The results in Fig. S9 are used to prove that the iron sublattice can withstand helium diffusion and therefore sustain the superionic phase. We first equilibrated FeHe at 10 TPa and 17,500 K. Next, we equilibrated at 19,000 K, a temperature at which helium melts and the relaxed temperature then decreases to 18,500 K. The iron sublattice survives for more than 1.5 ps, at which point we stop the simulation. We have performed additional tests in which the iron sublattice remains crystalline up to 10 ps. These molecular dynamics runs provide strong evidence for the existence of the superionic phase in FeHe.

It is interesting to note that the Lindemann criterion correctly predicts the existence of a superionic phase. This criterion associates nuclear vibrations with structural changes and states that a solid melts when the ratio of the root-mean-square nuclear vibrational amplitude and the interatomic separation exceeds some critical value,  $\sqrt{\langle u^2 \rangle}/a \gtrsim \lambda_c$ , which is usually taken to be  $\lambda_c = 0.1$ . The Lindemann criterion using the smallest He-He distance as the interatomic separation  $a$  predicts that the helium sublattice melts at temperatures of a few thousand Kelvin, but at those temperatures the Fe-Fe Lindemann ratio is significantly smaller than  $\lambda_c$ . These results suggest that, upon increasing temperature, the helium chains melt within the iron channels in FeHe before the iron channels themselves melt. We note that quantitatively, the Lindemann criterion results significantly deviate from the molecular dynamics results.

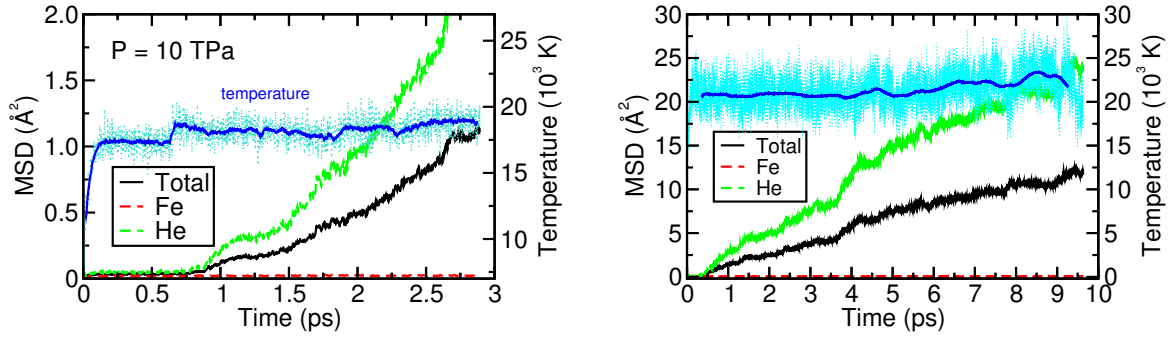


FIG. S9. Molecular dynamics runs of *Cmc* FeHe in which the helium sublattice is melted but the iron sublattice is not, demonstrating the existence of a superionic phase in FeHe.

### HELIUM AND IRON MELTING

We have calculated the helium melting curve using MD in a similar manner to that described above for FeHe *Cmc*. We will report full details of this calculation in a separate publication.

The iron melting curve is taken from Ref. [S36], in which density functional theory in conjunction with a two-phase coexistence approach was used.